4

OPTIMIZATION OF CdS AND CdSe QDSSCs WITH QDs PREPARED BY SUCCESSIVE IONIC LAYER ADSORPTION AND REACTION (SILAR)*

4.1 Introduction

The crucial process in the fabrication of a QDSSC is attaching the QDs onto a wide bandgap meso/nanoporous semiconducting film. QD synthesis and surface adsorption can be achieved via several routes [1]. The most common route is the wet chemical process such as chemical bath deposition (CBD) [2,3] and successive ionic layer adsorption and reaction (SILAR) [4,5]. Between these two methods, SILAR appears to be an easier and effective route to fabricate QD sensitizers. This technique has been widely used to fabricate CdS and CdSe QDs due to its simplicity [5a,6]. It has the advantage of depositing QDs with controlled size and volume by varying the

* Portion of this chapter were published in: Jun, H.K., Careem, M.A., & Arof, A.K. (2014). Fabrication, characterization and optimization of CdS and CdSe quantum dot-sensitized solar cells with quantum dots prepared by successive ionic layer adsorption and reaction. *International Journal of Photoenergy*, Volume 2014, Article ID 939423, 14 pages.

parameters such as precursor concentration (cationic and anionic solution), number of dipping cycles and dipping time. However, there are not many reports on the fabrication of CdSe QDs using SILAR route and this gives motivation to the undertaking of this study. Different parameters used appear to give different cell performances [7-10]. So far, there has not been any study reported on the optimization of SILAR method to deposit CdSe QDs on the TiO_2 semiconducting layer.

In this study, SILAR method was used to deposit CdS and CdSe QDs on TiO_2 surface which has been chosen as the base material in the photoanode. The processing parameters to fabricate QDs were varied in order to obtain solar cell performance of optimum efficiency. The parameters varied were concentration of precursor solutions, number of SILAR cycles and dipping time in each solution. Optimum parameter settings for the synthesis of CdS and CdSe QDs by SILAR method are anticipated.

CdS and CdSe QDs were deposited on TiO_2 surface of the working electrode using the SILAR technique as described in Chapter 3. Appropriate cationic and anionic precursor solutions were prepared prior to the depositions of QDs. The QDs prepared are referred to as CdS(*n*) and CdSe(*n*) respectively, where *n* is the number of SILAR cycles used for preparing them. Polysulfide electrolyte solution for use in CdS QDSSCs was prepared by dissolving 0.5 M Na_2S, 2 M S and 0.2 M KCl in methanol/water (7:3/v:v) following the work by Lee *et al.* [11]. This polysulfide electrolyte was reported to be suitable for CdS QDSSC. For CdSe QDSSCs, the polysulfide electrolyte solution was prepared from 0.6 M Na_2S, 0.2 M S and 0.2 M KCl in water/ethanol (7:3/v:v) as in reference [7]. The polysulfide was chosen as CdSe QDSSC using it has reported a higher performance. Characterization works were performed as per procedure in section 3.4, Chapter 3.

4.2 Results and discussion

4.2.1 SILAR method for preparing QDs

In this study, SILAR method has been used to fabricate CdS and CdSe QDs to sensitize the meso/nanoporous TiO_2 layers. The formation and growing of the semiconductor QD on the TiO_2 surface can be observed from the gradual colour changes taking place. As the number of SILAR cycles increased, the colour changed from lighter to darker shades. This change signifies the quantum confinement effects of the growing QDs [7]. Figure 4.1 shows the gradual colour changes of CdS and CdSe-sensitized TiO_2 films after successive increase of dipping cycles. The CdS QDs were prepared using 0.10 M precursor solutions with a dipping time of 5 min in each dipping. For the preparation of CdSe QDs 0.03 M precursor solutions were used and each dipping was set for 30 s. For CdS, a yellow-coloured film was obtained while in CdSe, the colour changes were very distinct as the SILAR cycle increased. With increasing SILAR cycles of CdSe deposition, the TiO_2 film surface turned dark. This simple deposition and growth of QDs provide an easy and controllable way for the fabrication of semiconductor-sensitized photoelectrodes.

The same colour changes were also observed with increasing precursor concentration or dipping time for a fixed number of dipping cycles. However, at higher concentrations or longer dipping times, the colour change was not as distinct as that observed with the increase in number of SILAR cycles. This observation will be explained in the following section.

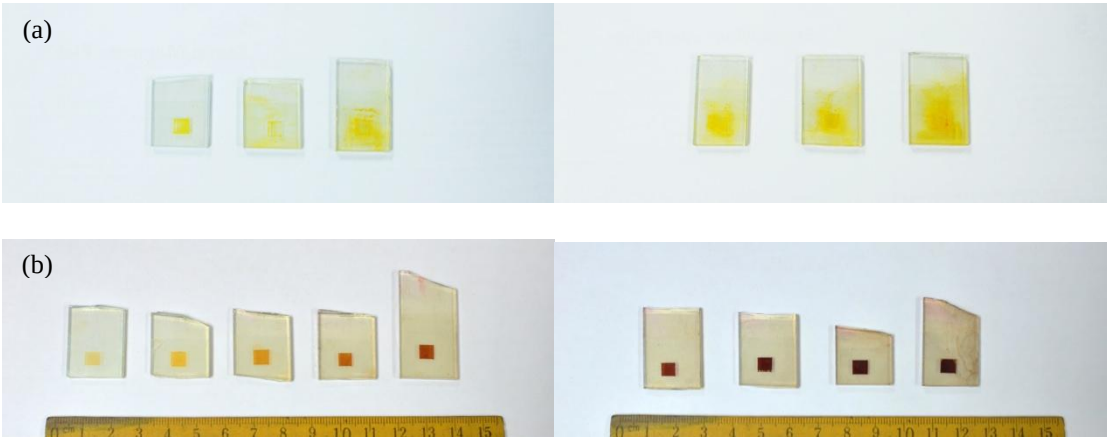

Figure 4.1 Photos of electrodes after each SILAR cycle (a) of 1-3, 5,7 and 10 cycles for CdS growth and (b) of 1-5, 7-10 cycles for CdSe growth.

4.2.2 Optimum concentration for precursor solutions

4.2.2.1 CdS QDs

Four different precursor concentrations were used for the fabrication of CdS and CdSe QDs. For CdS QD, concentrations of 0.05 M, 0.10 M. 0.50 M and 1.00 M were used for both anion and cation precursors. Photoelectrodes were prepared using 4 dipping cycles with a dipping time of 5 min in each solution. Figure 4.2(a) shows the optical absorbance of the CdS QD-sensitized electrode prepared in a set of precursor solutions having different concentrations. It can be seen that the absorption edge shifts to higher wavelengths as the concentration of the precursor is increased. However, the absorption edge is not well defined for the 1.00 M concentration. The adsorption edge wavelength for the precursor concentration of 0.05 M, 0.10 M and 0.50 M increased from 520 nm to 540 nm approximately suggesting a red-shift effect.

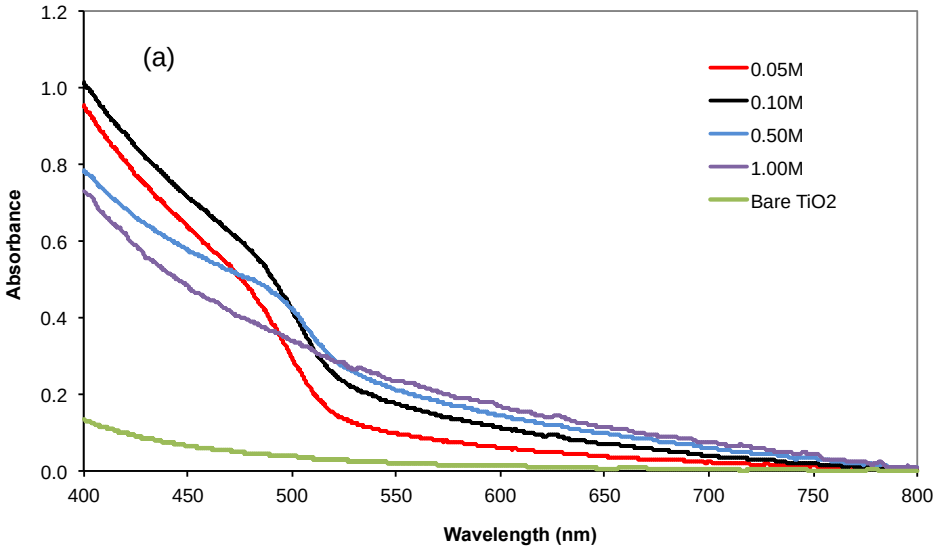

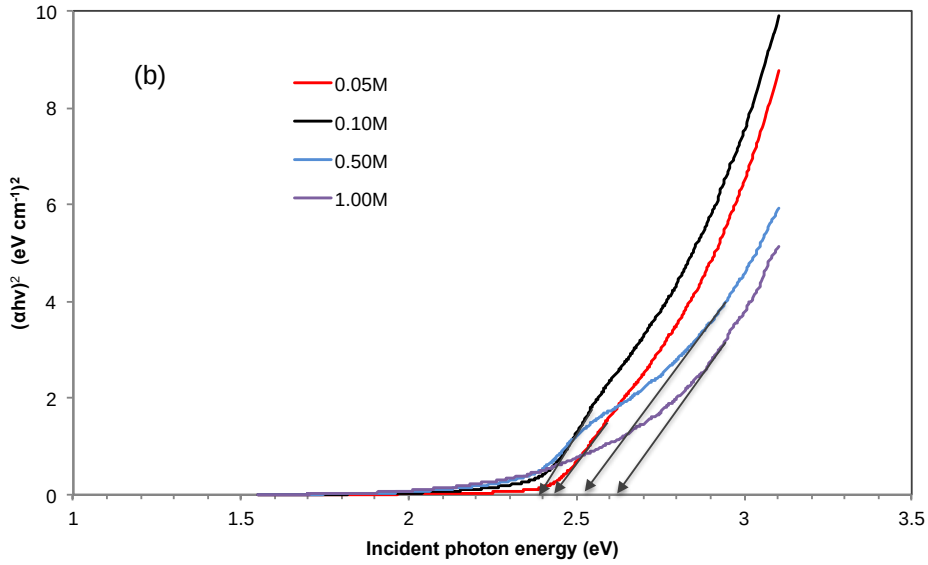

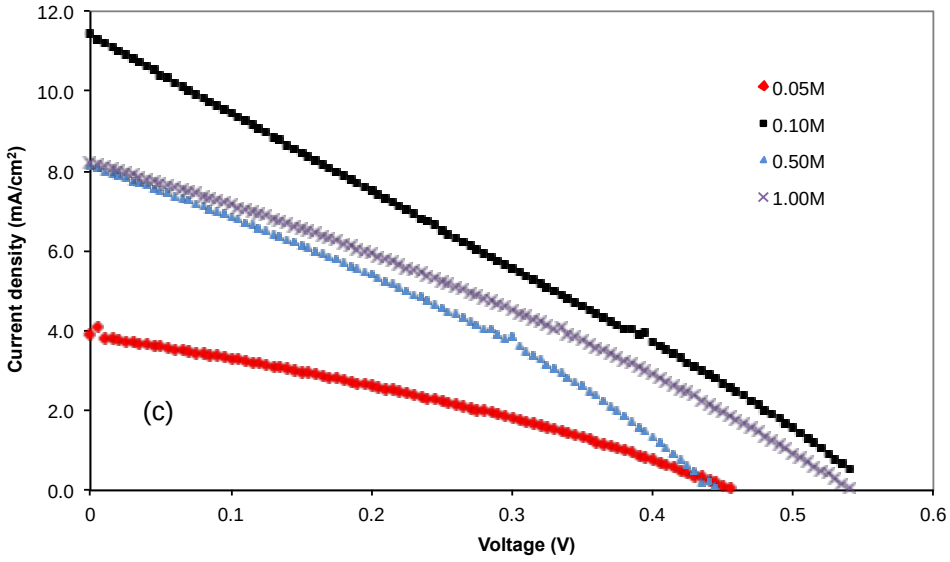

Figure 4.2 (a) UV-vis spectra, (b) Tauc plot, and (c) *J-V* curves of QDSSCs for CdS QDs prepared using different precursor concentrations.

Band gap energy of the QDs was estimated from Tauc plot, in which $(\alpha h\nu)^2$ against incident photon energy, $h\nu$ was plotted [12-14]. Here α is the absorbance value, h is the Planck's constant and ν is the frequency of the incident photon. The incident photon energy at a specific wavelength could be calculated as (1241.5×10^{-9}/ wavelength). The Tauc plot for CdS QDs is shown in Figure 4.2(b). The band gap energy of the QD sensitizer layer is obtained by extrapolating the straight line portion to the horizontal axis. Except for 0.10 M, the band gap energy increased with the increase of precursor concentration. This suggests that a smaller QD particle size can be obtained with higher precursor concentration. The size of the QDs can be estimated using Brus Equation [15-17]:

$$\Delta E = E_1 - E_g = (h^2/8r^2)\,(1/m_e + 1/m_h) \qquad (4.1)$$

where ΔE is the band gap energy shift, E_1 is the band gap of the QD, E_g is the band gap of the bulk materials, r is the radius of the QD, h is the Plank's constant, and m_e and m_h are the effective masses of electron and hole respectively. For CdS material, $m_e = 0.19\ m_o$, $m_h = 0.80\ m_o$ ($m_o = 9.11 \times 10^{-31}$ kg) and $E_g = 2.25$ eV [18], while for CdSe material, $m_e = 0.13\ m_o$, $m_h = 0.44\ m_o$ ($m_o = 9.11 \times 10^{-31}$ kg) and $E_g = 1.7$ eV [17]. Generally, in crystals, as the grain size increases, the band gap energy is reduced.

Fig. 4.2(c) shows the *J-V* curves obtained for QDSSCs fabricated with CdS QDs prepared using precursor solutions having different concentrations. The solar cell parameters obtained from these curves are listed in Table 4.1. The estimated band gaps and the diameters for the QDs are also indicated in this table.

Table 4.1 The energy gap and size of QDs and QDSSC performance parameters for CdS QDs prepared using different precursor concentrations.

Precursor concentration	QD band gap (eV)	Estimated QD diameter (nm)	J_{SC} (mA/cm^2)	V_{OC} (V)	Fill factor (%)	Efficiency, η (%)
0.05 M	2.43	7.4	3.90	0.455	31.6	0.56
0.10 M	2.38	8.6	11.42	0.565	25.9	1.67
0.50 M	2.53	5.9	8.12	0.445	32.0	1.16
1.00 M	2.63	5.1	8.21	0.540	31.0	1.37

It is interesting to note that the CdS QD prepared from high precursor concentration does not show the highest cell efficiency. In fact, the highest efficiency is observed when CdS QDs were prepared from precursor concentration of 0.10 M. The corresponding efficiency obtained is 1.67%. The QDs prepared from 0.10 M precursor concentration have the largest estimated QD size among the samples which corresponds to the lowest band gap energy. The diameter of the QDs which is estimated using equation (4.1) is 8.6 nm. When the precursor concentration is high, a large number of QD nuclei are formed on the TiO_2. As a result, more nano-sized QD particles are formed creating an overcrowding environment [17].

Therefore, with higher concentrations, it is suspected that the efficiency is limited due to the overloading of QDs on the top part of the TiO_2 layer. QDs will tend to form aggregates near the top of the TiO_2 film which will block the path for subsequent deposition of QDs in the deeper region of the film [17,19]. As a result, QDs deposition will continue to take place on the top surface only and the easy electron transfer from QD to the TiO_2 surface will be obstructed, leading to low current generation and hence low efficiency. Fill factor of the QDSSC does not change much with various concentrations as it depends on the resistance within the cell which is mainly determined by the redox electrolyte used and its contact with QDs and counter electrode.

The fill factor values obtained are below 32% which suggest the limitation of the cell performance unless the parameters are improved.

4.2.2.2 CdSe QDs

For CdSe QD preparation, 0.01 M, 0.03 M, 0.05 M and 0.10 M precursor concentrations were used. The photoelectrodes were prepared using 6 dipping cycles with a dipping time of 30 s. Figure 4.3(a) shows the UV-vis spectra of the CdSe QDs prepared from the four different precursor concentrations. The *J-V* curves of the CdSe QDSSCs with QDs prepared from four different precursor concentrations are shown in Figure 4.3(c) and Table 4.2 summarizes the band gap energy and QD size together with the corresponding cell performance parameters.

It is clearly seen that QDs prepared from 0.03 M concentration have the highest absorbance although QDs prepared using 0.05 M and 0.10 M solutions have higher absorption edges (around 700 nm compared to 610 nm of 0.03 M). Nevertheless, with higher concentrations, the absorption edge does shift to higher wavelength (in this case it is 700 nm). CdSe QDs prepared from 0.03 M precursor concentration also has the lowest band gap energy and highest QD size when compared with those obtained with other concentrations. The lowest band gap energy, which is 2.15 eV is favourable for electron conduction when excited as it only requires less energy for electron excitation. This value is quite near to the bulk energy band gap of CdSe (1.7 eV). The estimated diameter of QDs prepared from precursor concentration of 0.03 M is about 6.0 nm. The Tauc plots which give the approximate band gap energies are shown in Figure 4.3(b).

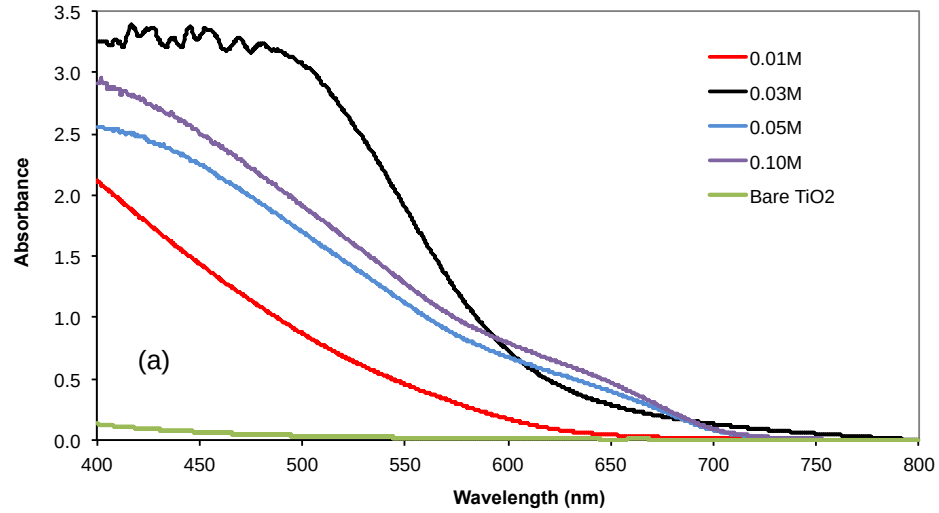

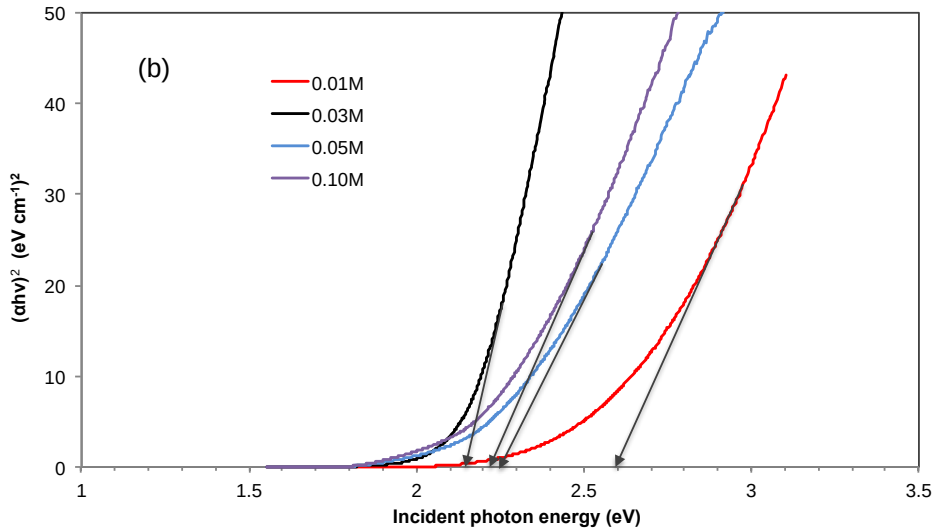

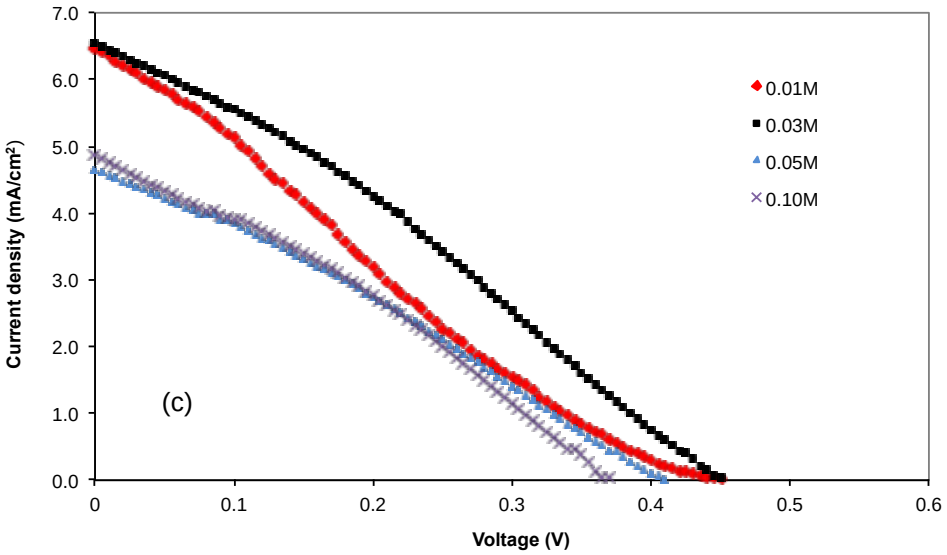

Figure 4.3 (a) UV-vis spectra, (b) Tauc plot, and (c) *J-V* curves of QDSSCs for CdSe QDs prepared using different precursor concentrations.

Table 4.2 The energy gap and size of QDs and QDSSC performance parameters for CdSe QDs prepared using different precursor concentrations

Precursor concentration	Band gap energy (eV)	Estimated QD diameter (nm)	J_{SC} (mA/cm^2)	V_{OC} (V)	Fill factor (%)	Efficiency, η (%)
0.01 M	2.60	4.2	6.47	0.450	23.0	0.67
0.03 M	2.15	6.0	6.55	0.450	31.0	0.91
0.05 M	2.25	5.4	4.66	0.410	29.0	0.55
0.10 M	2.23	5.5	4.87	0.370	31.0	0.56

Largest QDs with the lowest band gap energy give the highest QDSSC efficiency of 0.91 % with a fill factor of 31%. The performance of the cells does not improve with higher precursor concentrations. This could be due to formation of QD aggregates on the top surface of the TiO_2 film as explained above. Consequently, the short-circuit photocurrent density appears to be low.

4.2.3 Dipping cycles

The optimum precursor concentrations found in section 4.2.2 were selected for the next set of experiments in order to determine the number of SILAR dipping cycles needed to prepare QDs that would produce the best performance in QDSSCs. In the case of CdS and CdSe QDs, the precursor concentration of 0.10 M and 0.03 M that gave the optimum results, respectively were chosen for the experiments.

4.2.3.1 CdS QDs

For CdS QDs, SILAR dipping cycles ranging from 1 to 10 cycles were used with precursor concentration of 0.10 M. Dipping time in each solution was fixed at 5 min. QDs were prepared using 1-5, 7 and 10 SILAR cycles and their respective UV-

vis absorbance and QDSSCs were studied. As seen from the UV-vis spectra result (Figure 4.4(a)), the absorption edge shifts to higher wavelengths with increasing number of dipping cycles up to 4 cycles and remains almost fixed with further increase in number of dipping cycles. This could be linked to the number of QDs and their size on the TiO_2 surface. As the number of cycles increased, QDs begin to form mostly on the top surface of TiO_2 layer and their number and size increase gradually and may block the growth of QDs in the inner regions of the TiO_2 layer. Further increment of dipping cycles will therefore create QDs of smaller sizes on top and increase the thickness of the QD layer. This will keep the absorption edge almost at the same wavelength but with increased amount of absorption.

The Tauc plots for band gap energy estimation for QDs are shown in Figure 4.4(b) while the *J-V* curves of the CdS QDSSCs with QDs prepared using different number of SILAR dipping cycles are shown in Figure 4.4(c). Table 4.3 displays the summary of the band gap energy and size of the QDs and performance parameters of the QDSSCs based on them.

The optimum performance was obtained for the QDSSC with QDs prepared using 4 dipping cycles. Band gap energy estimation shows an optimum value of 2.38 eV for the QDs prepared from 4 dipping cycles. As the number of dipping cycles is increased beyond 4 cycles, there was no further improvement in the band gap energy. As for the size of the QDs formed, increased dipping cycles would result in larger QD size. The largest diameter of 8.6 nm for the QDs was obtained for 4 dipping cycles. With further increment of the number of dipping cycles the average diameter of the QDs

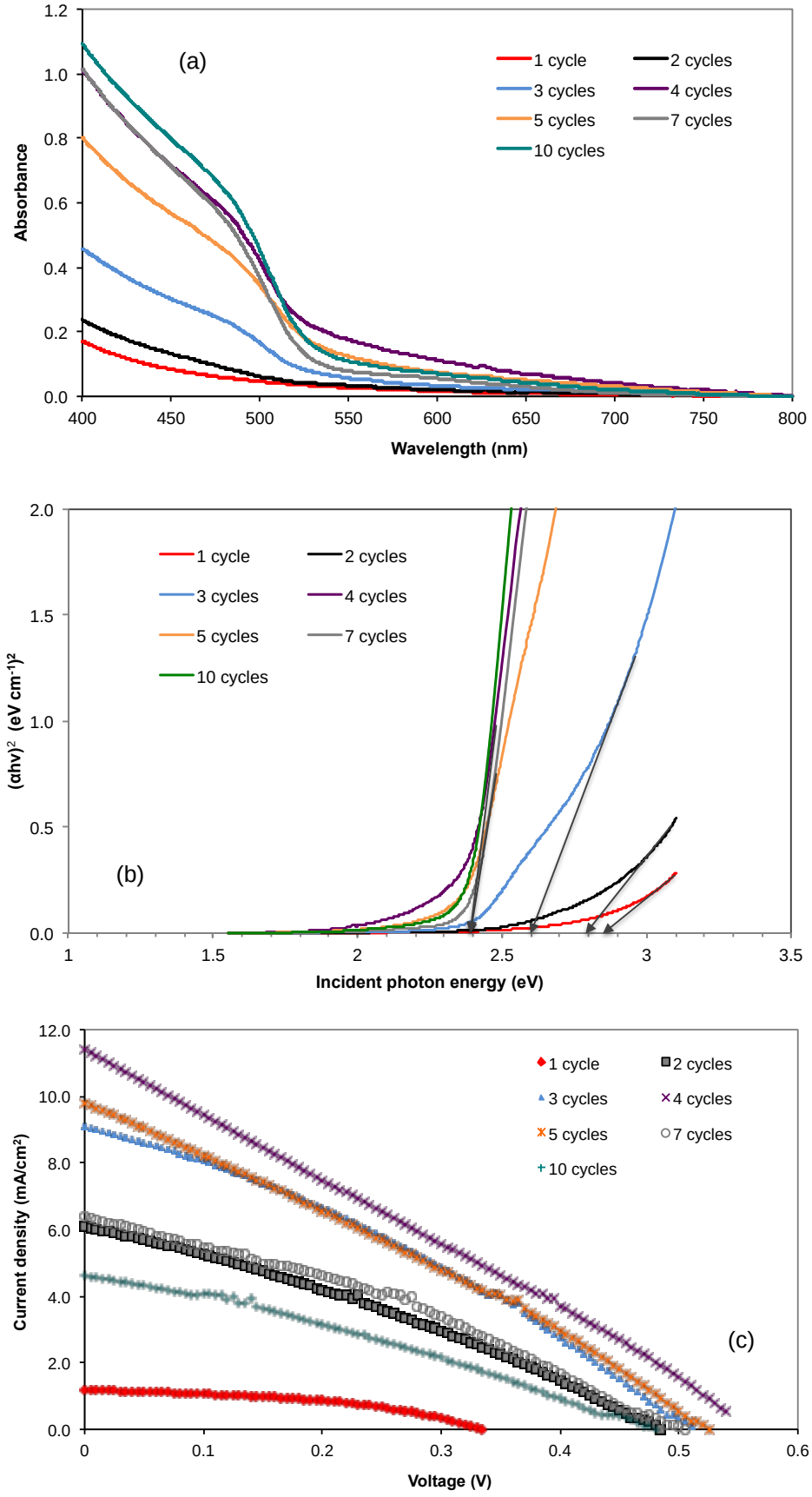

Figure 4.4 (a) UV-vis spectra, (b) Tauc plot, and (c) *J-V* curves of QDSSC for CdS QDs prepared using different number of SILAR cycles.

Table 4.3 The energy gap and size of QDs and QDSSC performance parameters for CdS QDs prepared from various SILAR cycles.

Number of dipping cycles	Band gap energy (eV)	Estimated QD diameter (nm)	J_{SC} (mA/cm^2)	V_{OC} (V)	Fill factor (%)	Efficiency, η (%)
1	2.85	4.0	1.18	0.335	44.3	0.18
2	2.80	4.2	6.09	0.485	31.6	0.93
3	2.60	5.3	9.10	0.510	31.7	1.47
4	2.38	8.6	11.42	0.565	25.9	1.67
5	2.40	8.1	9.80	0.525	28.1	1.45
7	2.40	8.1	6.37	0.505	33.8	1.09
10	2.40	8.1	4.62	0.480	30.1	0.67

remain same around 8 nm confirming that the size of QDs does not increase but smaller sized QDs are formed near the top of the TiO_2 layer instead. The QDSSC with QDs prepared using 4 dipping cycles produced the best overall cell performance with an efficiency of 1.67% with a fill factor of 25.9%.

4.2.3.2 CdSe QDs

For the CdSe QDs, optimum dipping solution concentration was found to be 0.03 M as shown in section 4.3.2.2. This solution concentration was used to prepare CdSe QDs using SILAR dipping cycles ranging from 1 to 10 cycles. Dipping time in each solution was fixed at 30 s. This period appears to be suitable for the dipping process as much shorter period does not give sufficient time for the QDs formation on the photoanode. Figure 4.5(a) shows the UV-vis spectra for CdSe QD-sensitized electrodes prepared from different number of dipping cycles while Figure 4.5(b) shows the corresponding $(\alpha h\nu)^2$ vs $h\nu$ plots for band gap energy estimation. Similar to the observation with CdS QD electrodes, the absorption edge shifts to higher wavelengths as the number of dipping cycle is increased and reaches optimum at 7 cycles. From the

band gap energy estimation, the estimated band gap energy for QDs obtained from 7 dipping cycles is 2.17 eV. The corresponding diameter of such QDs is 5.9 nm.

Figure 4.5(c) shows the *J-V* curves for the CdSe QDSSCs with QDs prepared using different number of dipping cycles while the performance parameters of the cells with the estimated energy gaps and size of QDs are tabulated in Table 4.4. As the number of cycles increases the performance parameters increase, reach maximum values for 7 cycles before decrease. The CdSe QDSSC with CdSe QDs prepared using 6 dipping cycles does not show the highest efficiency although the QDs have the somewhat lower band gap energy. The best efficiency of 1.21% with fill factor of 28% is observed for the cell with CdSe QDs prepared from 7 dipping cycles. The corresponding QDs have lower band gap energy with estimated QD size of 5.9 nm in diameter. At 7 dipping cycles, the TiO_2 surface could have been attached with CdSe QDs optimally, giving rise to the maximum current density of the cell. When the number of dipping cycles is increased further, the efficiency decreases. This result shows that more dipping cycles do not contribute to higher performance. The poor performance of the QDSSCs with QDs prepared from large number of dipping cycles can be attributed to the overloading of the QDs on the top part of the TiO_2 layer as in the case of CdS QDSSC. This is further illustrated by the increase in size of the QDs and decrease of the photocurrent density for QDs prepared with more than 7 cycles.

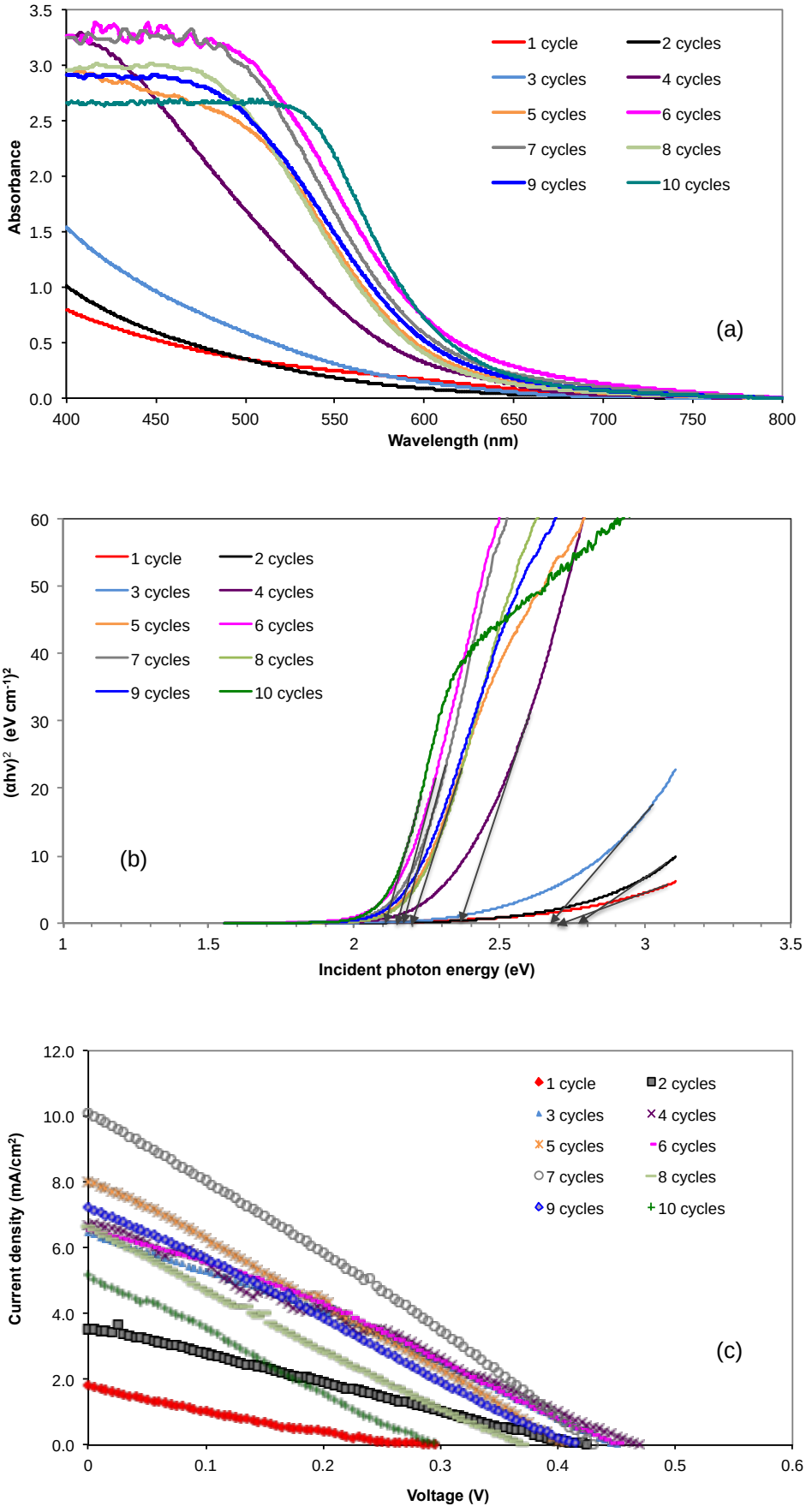

Figure 4.5 (a) UV-vis spectra, (b) Tauc plot, and (c) *J-V* curves of QDSSC for CdSe QDs prepared using different number of dipping cycles.

Table 4.4 The energy gap and size of QDs and QDSSC performance parameters for CdSe QDs prepared using different number of dipping cycles.

Number of dipping cycles	Band gap energy (eV)	Estimated QD diameter (nm)	J_{SC} (mA/cm^2)	V_{OC} (V)	Fill factor (%)	Efficiency, η (%)
1	2.70	3.9	1.80	0.295	20.0	0.11
2	2.77	3.8	3.55	0.425	25.0	0.38
3	2.67	4.0	6.44	0.450	30.0	0.87
4	2.37	4.9	6.70	0.470	28.0	0.88
5	2.17	5.9	8.04	0.405	27.0	0.88
6	2.15	6.0	6.55	0.450	31.0	0.91
7	2.17	5.9	10.09	0.430	28.0	1.21
8	2.20	5.7	6.63	0.370	25.0	0.61
9	2.16	6.0	7.23	0.415	26.0	0.78
10	2.11	6.3	5.16	0.295	25.0	0.38

4.2.4 Dipping time

The third parameter which is important is the dipping time in each solution. This parameter goes hand in hand with the number of dipping cycles as longer dipping time would require lesser number of dipping cycles and vice versa. Likewise, QDSSC performance may vary depending on the dipping time and the number of dipping cycles during the QD preparation. The optimum numbers of dipping cycles as determined in section 4.2.3 were used for the preparation of CdS and CdSe QDs in this study.

4.2.4.1 CdS QDs

The CdS QDs coated electrodes were prepared from solutions having 0.10 M concentration (both anion and cation solutions) and 4 dipping cycles with dipping time for each solution ranging from 1 min to 10 min. UV-vis spectra for the

CdS QD electrodes prepared using different dipping times are shown in Figure 4.6(a) and Figure 4.6(b) displays the corresponding Tauc plots for band gap energy estimation. As can be seen the absorption edge shifts to higher wavelengths with increasing dipping time reaching a maximum wavelength and then shifts to lower wavelengths with further increase in dipping time. The optimum absorption edge is observed for the electrode prepared with 5 min dipping time in each anion and cation solutions. This corresponds to a band gap energy of 2.38 eV, which is the lowest within the group. The estimated QD size for this band gap energy is 8.6 nm.

J-V curves of the QDSSCs with QDs prepared using different dipping times are shown in Figure 4.6(c). Table 4.5 shows the summary of the QD band gap energies and the performance parameters for the QDSSCs. The estimated diameters of the QDs are also shown in this Table.

The efficiency of the QDSSC with QDs prepared using 5 min dipping time per solution shows the highest efficiency at 1.67% with a fill factor of 25.9%. Shorter dipping times could not produce high efficiency due to the resulting low number of QDs or smaller sized QDs deposited on the TiO_2 surface. Longer dipping times produce too many QDs of smaller sizes as in the case of 8 min or larger size QDs as in the case of 10 min which overcrowd the TiO_2 surface and prevent the easy electron transfer from QDs toTiO_2. Subsequently, the efficiency is affected by the QD loading.

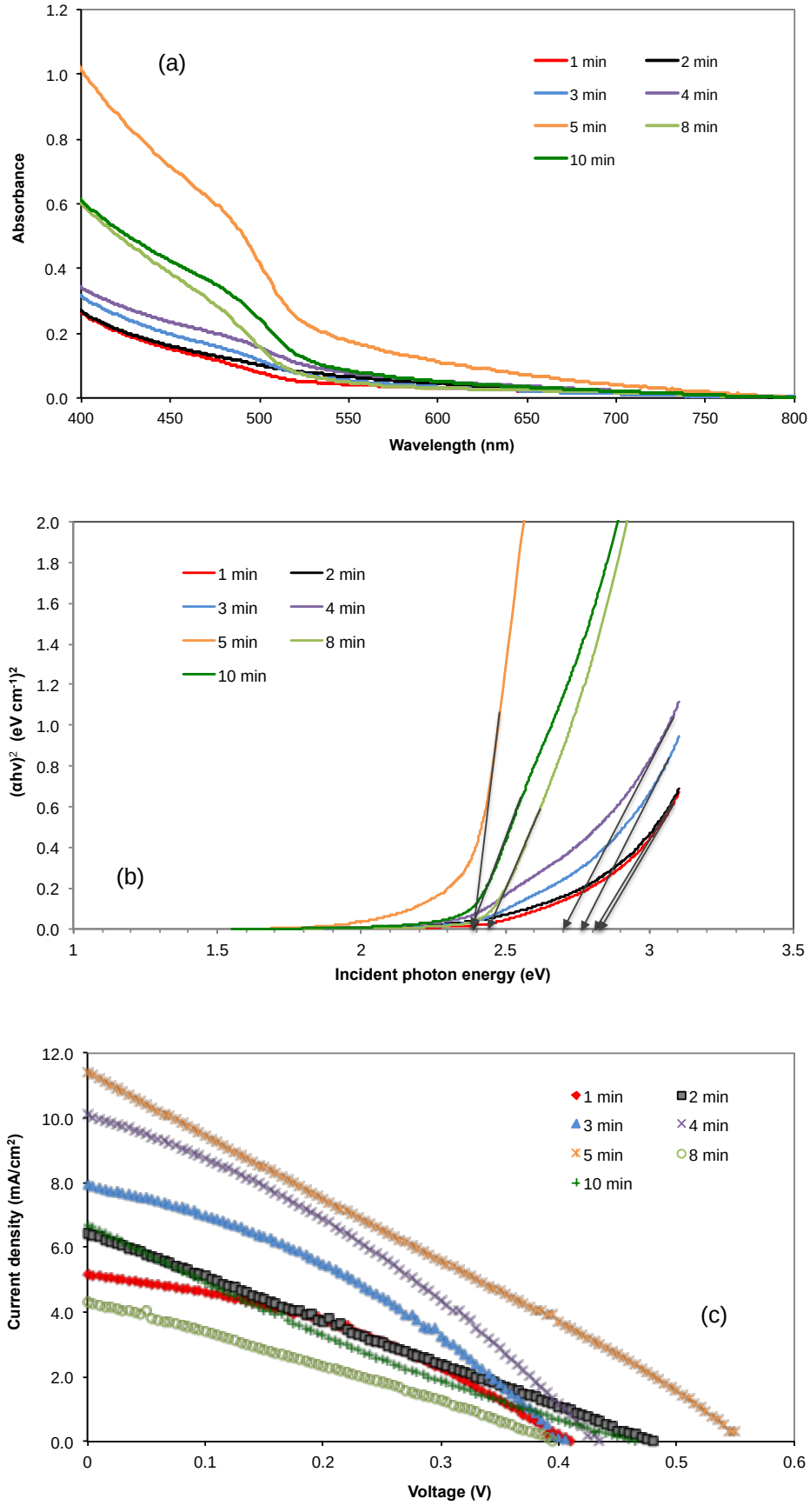

Figure 4.6 (a) UV-vis spectra, (b) Tauc plot, and (c) *J-V* curves of QDSSC for CdS QDs prepared using different dipping times.

Table 4.5 The energy gap and size of QDs and QDSSC performance parameters for CdS QDs prepared using various dipping times.

Dipping time	Band gap energy (eV)	Estimated QD diameter (nm)	J_{SC} (mA/cm^2)	V_{OC} (V)	Fill factor (%)	Efficiency, η (%)
1 min	2.84	4.1	5.15	0.410	37.5	0.79
2 min	2.82	4.1	6.43	0.480	25.5	0.79
3 min	2.77	4.3	7.92	0.405	35.1	1.13
4 min	2.70	4.7	10.09	0.435	32.5	1.43
5 min	2.38	8.6	11.42	0.565	25.9	1.67
8 min	2.45	7.0	4.31	0.395	27.7	0.47
10 min	2.38	8.6	6.70	0.465	21.1	0.66

4.2.4.2 CdSe QDs

CdSe QD deposited electrodes were prepared form the solution having the optimum concentration of 0.03 M using 7 dipping cycles with various dipping times for each solution ranging from 30 s to 150 s. The absorbance spectra of the electrodes and the corresponding Tauc plots for band gap energy estimation are shown in Figure 4.7(a) and Figure 4.7(b) respectively. As the dipping time is increased, the absorption edge of the corresponding electrode shifts to the red wavelength region. The lowest band gap energy (largest QD size) is obtained with a dipping time of 90 s. The *J-V* curves for the QDSSCs with QDs prepared with different dipping times are shown in Figure 4.7(c) and their performance parameters and band gaps and size of the QDs are given in Table 4.6. The efficiency of the cells decreases with the increase in the dipping time (after 30 s). The poor performance of the cells with QDs prepared with longer dipping times could be attributed to the excessive QD aggregation on the TiO_2 surface which increases the resistance for electron transfer. The best efficiency of 1.21% is obtained for the cell prepared with QDs using 30 s dipping time.

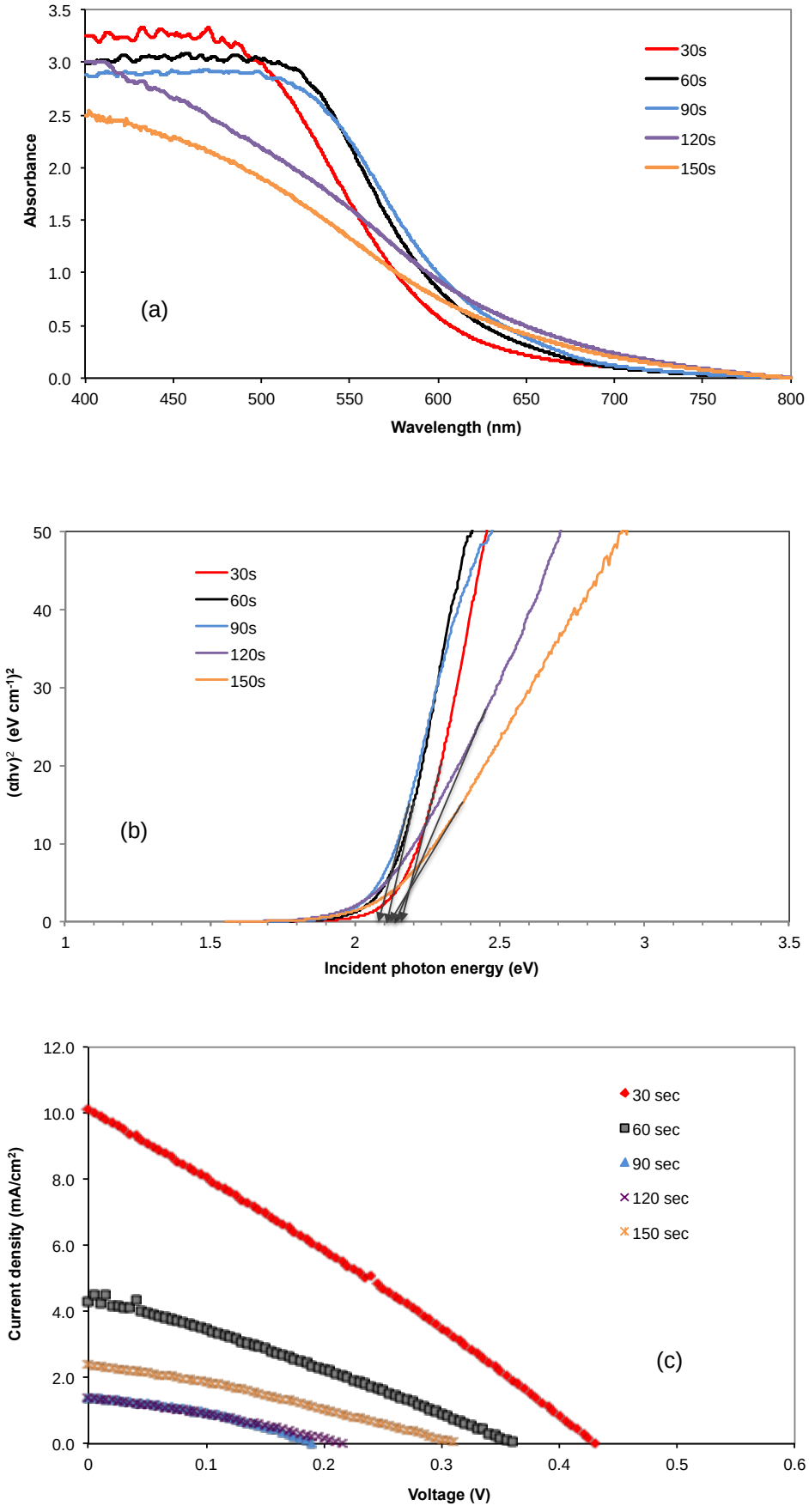

Figure 4.7 (a) UV-vis spectra, (b) Tauc plot, and (c) *J-V* curves of QDSSCs for CdSe QDs prepared using different dipping times.

Table 4.6 The energy gap and size of QDs and QDSSC performance parameters for CdSe QDs prepared using various dipping times.

Dipping time	Band gap energy (eV)	Estimated QD diameter (nm)	J_{SC} (mA/cm^2)	V_{OC} (V)	Fill factor (%)	Efficiency, η (%)
30 s	2.17	5.9	10.09	0.430	28.0	1.21
60 s	2.12	6.3	4.33	0.360	29.0	0.45
90 s	2.08	6.6	1.41	0.190	36.0	0.10
120 s	2.15	6.0	1.40	0.215	31.0	0.09
150 s	2.13	6.2	2.38	0.310	30.0	0.22

Based on the results reported above, the most efficient CdS QDSSC can be fabricated with QDs prepared from precursor concentration of 0.10 M using 4 SILAR dipping cycles with 5 min dipping time in each solution. The estimated QD size is 8.6 nm in diameter and the band gap energy is 2.38 eV. For CdSe QDSSC, the best performance cell can be obtained with QDs prepared from precursor concentration of 0.03 M with 7 SILAR dipping cycles with a dipping time of 30 s in each solution. The estimated QD size for best performance is 5.9 nm in diameter and the band gap is 2.17 eV. The efficiency of the optimized CdS QDSSC is better than the reported results [5b,7,9]. However, the performance for CdSe QDSSC is far lower than the reported results in the literature [8]. This difference is attributed to the different photoanode setup that has been used in this work which did not include a ZnS passivation layer, a TiO_2 scattering layer, optimizing the thickness of the TiO_2 layer, etc. Throughout the study, it is observed that if any of the QD preparation parameters exceeded the optimum level, the resulting efficiency of the solar cell will be reduced due to overloading or formation of QD aggregates on top of the TiO_2 film surface. Also it is to be noted that CdSe QDs are difficult to attach on TiO_2 surface due to high tendency of forming inhomogeneous QD distribution on the TiO_2 surface [17]. Nevertheless, the results presented in this

study can be used as a guideline for the preparation of efficient CdS and CdSe QDSSCs with optimized electrolytes and TiO_2 layers.

4.2.5 Surface morphology of the optimized QD-sensitized electrode

The deposition and growth of CdS and CdSe QDs on TiO_2 films were observed with FESEM imaging. Figure 4.8 (a, c and e) shows the surface morphology of the TiO_2 film with and without QD deposition. With the deposited CdS and CdSe QDs, the TiO_2 particle size appears to be a little larger compared to that in the bare TiO_2 film. The slight change of particle size after deposition of QDs can be attributed to the formation and growth of the QDs on the TiO_2 surface. This observation agrees with the colour changes of the TiO_2 mesoporous surface as explained in section 4.2.1. The degree of porosity of the observed TiO_2 mesoporous surface was analyzed with *Image J* software [20]. In bare TiO_2, the degree of porosity is estimated to be 48.6%. After deposition of CdS QDs using 4 SILAR cycles, the degree of porosity reduced to 46.6% while for CdSe QDs deposited using 7 SILAR cycles, the estimated value is 43.0%. The reduction of the degree of porosity implies that the volume of TiO_2 particles have increased as a result of QDs deposition on the surface.

To further confirm the formation and growth of QDs on the TiO_2 film surface, the QD-deposited TiO_2 films were scratched off from the FTO glass and suspended in ethanol solution for HR-TEM studies. A droplet of the suspension was placed on a grid for HR-TEM viewing. Three samples were selected for HR-TEM analysis: bare TiO_2 film, CdS(4)-sensitized TiO_2 film and CdSe(7)-sensitized TiO_2 film. The observed lattice spacing was compared to the data in JCPDS. The HR-TEM images for each

sample are shown in Figure 8 (b, d and f). Lattice spacing of the particle is shown in the image as well. The QD elements are shown by EDX result in Figure 4.8 (g and h).

In bare TiO_2 film, a distinct d-spacing of about 0.36 nm is observed in grains having an average size of 25 nm. This d-value corresponds to the (101) plane of anatase TiO_2. For the QD-deposited TiO_2 film, CdS and CdSe particles are observed to be attached on the TiO_2 surface. In the CdS-deposited TiO_2 film, d-spacing of 0.205 nm which corresponds to the (220) plane of CdS QDs attached to a TiO_2 particle is observed. These CdS QDs have the size of 8.0 nm which is quite close to the approximate QD size obtained in the section 4.2.2.1. In the CdSe-deposited TiO_2 film sample, the CdSe QDs have a d-spacing of 0.329 nm. This corresponds to the (101) plane of CdSe. The estimated size of the QDs is in agreement with the QD size estimated earlier in section 4.2.2.2 which is about 5.9 nm.

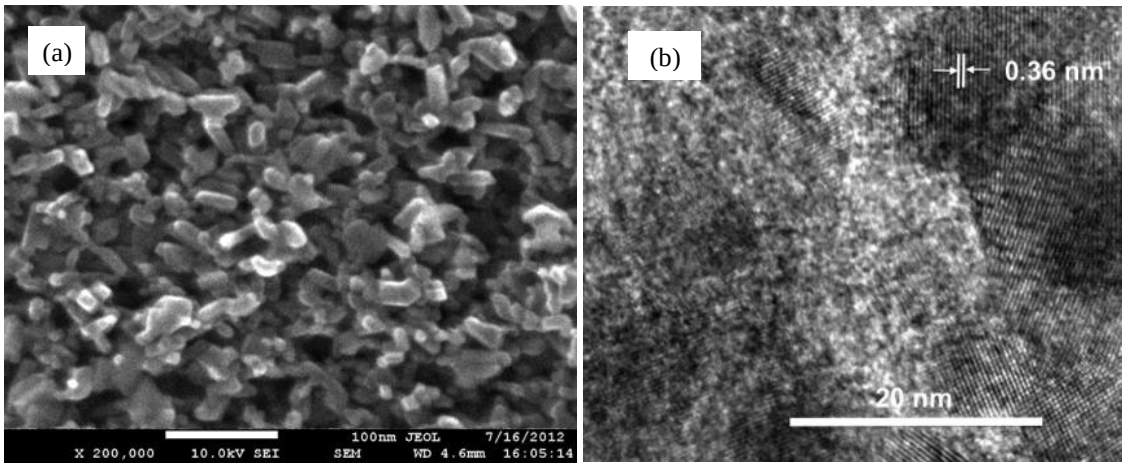

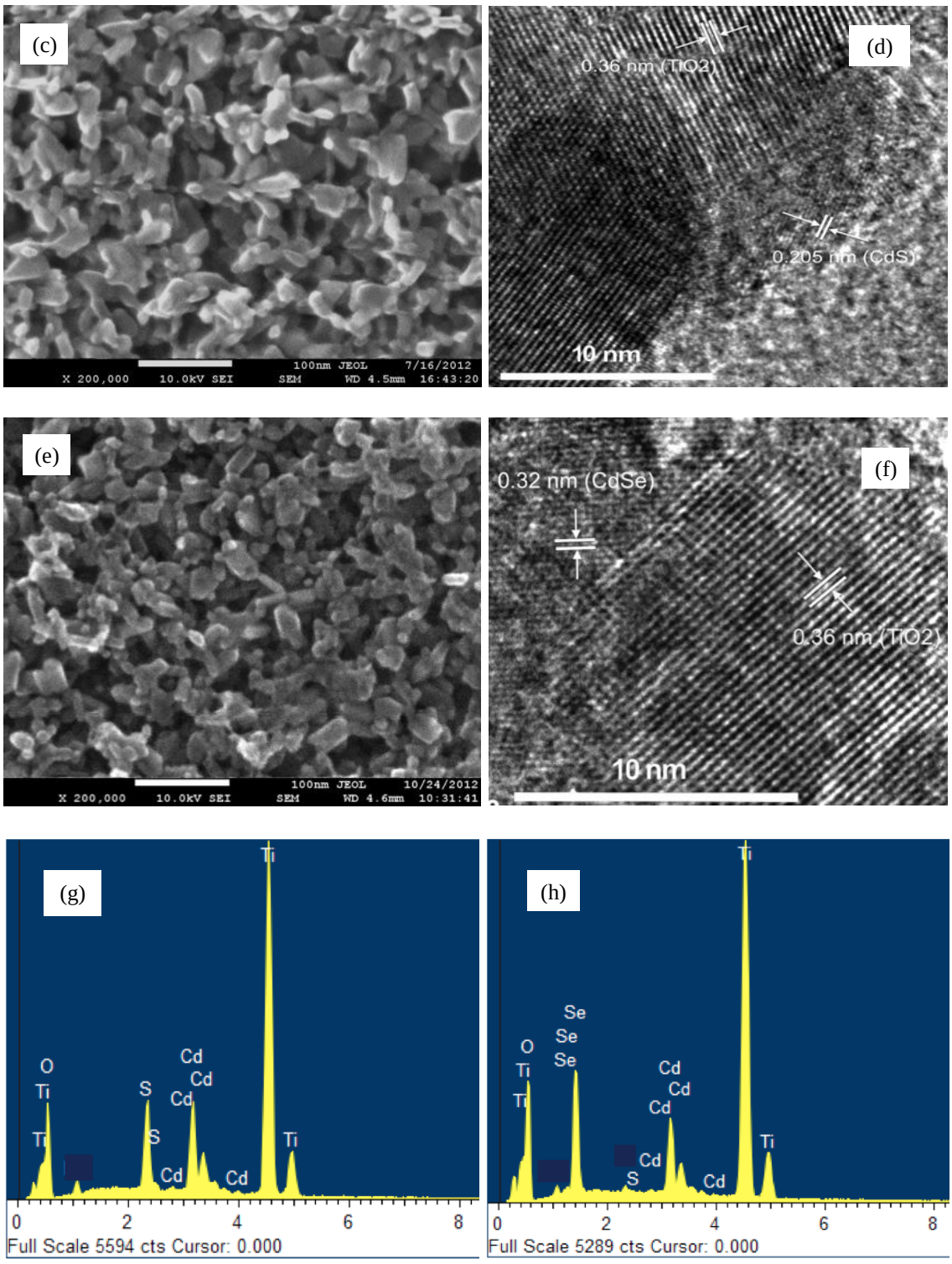

Figure 4.8 FESEM images of (a) bare TiO_2 film surface, (c) CdS(4)-sensitized TiO_2 film and (e) CdSe-sensitized TiO_2 film. TEM images of (b) bare TiO_2 film surface, (d) CdS(4)-sensitized TiO_2 film and (f) CdSe-sensitized TiO_2 film. EDX result of (g) CdS(4)-sensitized TiO_2 film and (h) CdSe-sensitized TiO_2 film.

4.3 Summary

CdS and CdSe quantum dot sensitized solar cells (QDSSCs) were fabricated using QDs prepared by SILAR method. Optimization study was performed on three quantum dot preparation parameters: concentration of precursor solutions, number of dipping cycles and dipping time in each solution. To achieve the best performance in CdS QDSSCs, QDs must be prepared from precursor solutions each having a concentration of 0.10 M with 4 SILAR dipping cycles and 5 min dipping time in each solution. For CdSe QDSSC, the optimum parameters for QD preparation are precursor solution concentration of 0.03 M and 7 dipping cycles with a dipping time of 30 s in each solution. The corresponding estimated QD diameter size for CdS and CdSe QDs are 8.6 nm and 5.9 nm respectively. These diameter values are quite close to the observed particle sizes using HR-TEM. The estimated band gap energy for the optimized CdS and CdSe QDs are 2.38 eV and 2.17 eV respectively. It is also observed that upon deposition of QDs, the TiO_2 particles size appears to increase resulting in a reduction of porosity. Further deposition of QDs results in overcrowding near the top of the TiO_2 base layer and reduces the short circuit current density in QDSSCs and thereby limit their performance. The optimized CdS and CdSe QDSSCs have efficiency of 1.67% and 1.21% respectively. Photocurrent density of the optimized CdS and CdSe QDSSC are 11.42 mA/cm^2 and 10.09 mA/cm^2 respectively. Although the performance of obtained in this study is low, especially for CdSe QDSSC, higher performance is possible when proper surface passivation technique, choice of counter electrode and optimum TiO_2 layer, to name a few, are applied. This study illustrates the importance of choosing the correct sized QDs and their distribution for optimizing the performance of QDSSCs.

4.4 References

[1] Emin, S., Singh, S.P., Han, L., Satoh, N., & Islam, A. (2011). Colloidal quantum dot solar cells. *Solar Energy,* 85, 1264-1282.

[2] Shen, Q., Arae, D., & Toyoda, T. (2004). Photosensitization of nanostructured TiO_2 with CdSe quantum dots: effects of microstructure and electron transport in TiO_2 substrate. *Journal of Photochemistry and Photobiology A: Chemistry,* 164, 75-80.

[3] Toyoda, T., Tsuboya, I., & Shen, Q. (2005). Effect of rutile-type content on nanostructured anatase-type TiO_2 electrode sensitized with CdSe quantum dots characterized with photoacoustic and photoelectrochemical current spectroscopies. *Materials Science and Engineering: C,* 25, 853-857.

[4] Pathan, H.M., & Lokhande, C.D. (2004). Deposition of metal chalcogenide thin films by successive ionic layer adsorption and reaction (SILAR) method. *Bulletin of Materials Science,* 27, 85-111.

[5] (a) Toyoda, T., Sato, J., & Shen, Q. (2003). Effect of sensitization by quantum-sized CdS on photoacoustic and photoelectrochemical current spectra of porous TiO_2 electrodes. *Review of Scientific Instruments,* 74, 297-299. (b) Tachibana, Y., Umekita, K., Otsuka, Y., & Kuwabata, S. (2008). Performance improvement of CdS quantum dots sensitized TiO_2 solar cells by introducing a dense TiO_2 blocking layer. *Journal of Physics D: Applied Physics,* 41, 102002.

[6] Barcelo, I., Lana-Villarreal, T., & Gomez, R. (2011). Efficient sensitization of ZnO nanoporous films with CdSe QDs grown by Successive Ionic Layer Adsorption and Reaction (SILAR). *Journal of Photochemistry and Photobiology A: Chemistry,* 220, 47-53.

[7] Lee, H.J., Bang, J., Park, J., Kin, S., & Park, S.-M. (2010). Multilayered semiconductor (CdS/CdSe/ZnS)-Sensitized TiO_2 mesoporous solar cells: All prepared by successive ionic layer adsorption and reaction processes. *Chemistry of Materials,* 22, 5636-5643.

[8] Lee, H.J., Wang, M., Chen, P., Gamelin, D.R., Zakeeruddin, S.M., Grätzel, M., *et al.* (2009). Efficient CdSe quantum dot-sensitized solar cells prepared by improved succesive ionic layer adsoprtion and reaction process. *Nano Letters,* 9, 4221-4227.

[9] Zewdu, T., Clifford, J.N., Hernandez, J.P., & Palomares, E. (2011). Photo-induced charge transfer dynamics in efficient TiO_2/CdS/CdSe sensitized solar cells. *Energy and Environmental Science,* 4, 4633-4638.

[10] Seo, M.-H., Hwang, W.-P., Kim, Y.-K., Lee, J.-K., & Kim, M.-R. (2011, June). *Improvement of quantum dot-sensitized solar cells based on Cds and CdSe quantum dots.* Paper presented at 37th IEEE Photovoltaic Specialists Conference (PVSC), Seattle, WA.

[11] Lee, Y.-L., & Chang, C.-H. (2008). Efficient polysulfide electrolyte for CdS quantum dot-sensitized solar cells. *Journal of Power Sources,* 185, 584-588.

[12] Tauc, J. (1968). Optical properties and electronic structure of amorphous Ge and Si. *Materials Research Bulletin,* 3, 37-46.

[13] Lee, W., Min, S.K., Dhas, V., Ogale, S.B., & Han, S.-H. (2009). Chemical bath deposition of CdS quantum dots on vertically aligned ZnO nanorods for quantum dots-sensitized solar cells. *Electrochemistry Communications,* 11, 103-106.

[14] Chen, H., Li, W., Liu, H., & Zhu, L. (2010). A suitable deposition method of CdS for high performance CdS-sensitized ZnO electrodes: Sequential chemical bath deposition. *Solar Energy,* 84, 1201-1207.

[15] Brus, L. (1986). Electronic wave functions in semiconductor clusters: experiment and theory. *Journal Physical Chemistry*, 90, 2555-2560.

[16] (a) Shen, Q., Kobayashi, J., Diguna, L.J., & Toyoda, T. (2008). Effect of ZnS coating on the photovoltaic properties of CdSe quantum dot-sensitized solar cells. *Journal of Applied Physics,* 103, 084304. (b) Shen, Q., & Toyoda, T. (2004). Characterization of nanostructured TiO_2 electrodes sensitized with CdSe quantum dots using photoacoustic and photoelectrochemical current methods. *Japanese Journal of Applied Physics,* 43, 2946-2951.

[17] Tian, J., Gao, R., Zhang, Q., Zhang, S., Li, Y., Lan, J., *et al.* (2012). Enhanced performance of CdS/CdSe quantum dot cosensitized solar cells via homogeneous distribution of quantum dots in TiO_2 film. *Journal of Physical Chemistry C,* 116, 18655-18662.

[18] Grätzel, M. (2001). Photoelectrochemical cells. *Nature,* 414, 338-344.

[19] Sudhagar, P., Jung, J.H., Park, S., Lee, Y.G., Sathyamoorthy, R., Kang, Y.S., *et al.* (2009). The performance of coupled (CdS:CdSe) quantum dot-sensitized TiO_2 nanofibrous solar cells. *Electrochemistry Communications,* 11, 2220-2224.

[20] Rasband, W.S. (1997-2012). *ImageJ*. Retrieved from U. S. National Institutes of Health, Bethesda, Maryland, USA, website: http://imagej.nih.gov/ij/